Accepted Manuscript

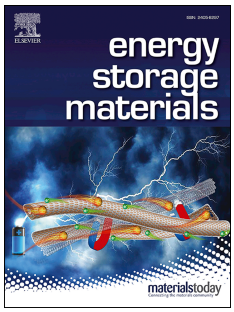

The Liquid Ammoniate of Sodium Iodide as an Alternative Electrolyte for Sodium Ion Batteries: the Case of Titanium Dioxide Nanotube Electrodes

Débora Ruiz-Martínez, Roberto Gómez

PII: S2405-8297(19)30896-7

DOI: https://doi.org/10.1016/j.ensm.2019.07.036

Reference: ENSM 861

To appear in: *Energy Storage Materials*

Received Date: 24 April 2019

Revised Date: 11 July 2019

Accepted Date: 24 July 2019

Please cite this article as: D. Ruiz-Martínez, R. Gómez, The Liquid Ammoniate of Sodium Iodide as an Alternative Electrolyte for Sodium Ion Batteries: the Case of Titanium Dioxide Nanotube Electrodes, *Energy Storage Materials*, https://doi.org/10.1016/j.ensm.2019.07.036.

TITLE PAGE

The Liquid Ammoniate of Sodium Iodide as an Alternative Electrolyte for Sodium Ion Batteries: the Case of Titanium Dioxide Nanotube Electrodes

Débora Ruiz-Martínez, Roberto Gómez*

Departament de Química Física i Institut Universitari d'Electroquímica, Universitat d'Alacant, Apartat 99, E-03080 Alicante, Spain

*Corresponding author.

Email address: Roberto.Gomez@ua.es (R. Gómez)

The Liquid Ammoniate of Sodium Iodide as an Alternative Electrolyte for Sodium Ion Batteries: the Case of Titanium Dioxide Nanotube Electrodes

ABSTRACT

Efforts for the development of sodium ion batteries (NIB) are focusing on insertion electrode materials rather than on novel electrolytes. In a radically new approach, sodium insertion into amorphous TiO_2 nanotubes, chosen as a typical electrode material for NIBs, is studied for the NaI liquid ammoniate ($NaI \cdot 3.3NH_3$) and compared with the behavior in typical organic electrolytes (for instance 1 M $NaClO_4$ in propylene carbonate, PC). The liquid ammoniate leads to significantly larger electrode capacities (between 0.5 and 2.6 V vs. Na^+/Na): 145 $mA \cdot h \cdot g^{-1}$ in $NaI \cdot 3.3NH_3$ versus 105 $mA \cdot h \cdot g^{-1}$ in $NaClO_4$/PC at 1 $mA \cdot cm^{-2}$ (14C for the ammoniate). This is linked to the outstanding conductivity and sodium concentration of $NaI \cdot 3.3NH_3$, together with the much smaller charge transfer resistance observed for this electrolyte. In more general vein, the prospects for using the $NaI \cdot 3.3NH_3$ liquid ammoniate in NIBs are finally discussed.

KEYWORDS: titanium dioxide, amorphous nanotubes, inorganic electrolytes, ammonia solvates, sodium ion batteries

. **ABBREVIATIONS:**

NIB: sodium ion battery.

NT: Nanotube.

PC: propylene carbonate.

EIS: electrochemical impedance spectroscopy.

1. Introduction

One of the challenges faced by mankind is finding efficient and cost-effective energy storage systems and devices. Among the different ways of storing energy, batteries and accumulators offer the advantage of having energy efficiencies unrivaled by other technologies [1–4]. The relative scarcity and high cost of lithium, upon which the most popular batteries for mobile applications are based [5–7], may hinder a further penetration of this technology. One obvious way forward relies on the substitution of lithium by sodium [8–11]. During the last years, several efforts have been realized to identify novel electrolytes for sodium batteries. Apart from the typical organic solutions based on aprotic solvents such as propylene carbonate, some studies have considered the use of sodium-based ionic liquids [12–18], which have the disadvantage of a relatively low conductivity limiting the development of high power density devices. We have recently introduced three different liquid solvates based on ammonia for their use in rechargeable Na metal batteries. These electrolytes are closely connected with ionic liquids [19]. They are known as liquid ammoniates and present a high sodium ion concentration (above 7M) and a high specific conductivity (values around 100 $mS \cdot cm^{-1}$). They allow for an exceedingly reversible behavior for the Na^+/Na redox couple at and below room temperature. Among ammonia solvates, the sodium iodide ammoniate $NaI \cdot 3.3NH_3$ has the practical advantage of a relatively low volatility. In fact, a few decades ago, this electrolyte was introduced for the preparation of sodium metal primary batteries using transition metal oxides (CuO and MnO_2) as cathodes [20].

In view of the excellent electrochemical behavior of metallic sodium in the aforementioned electrolytes, we want to show in this article how liquid ammoniates

could also represent a breakthrough for NIBs. An effective way for achieving this goal is based on a comparison of the behavior of well-defined electrode materials for sodium insertion in the ammoniate and in a typical organic electrolyte. It is worth noting that a significant effort is being done in the last years aiming at the development of effective and affordable electrode materials for sodium ion batteries. In such a context, and among the various materials proposed for sodium ion batteries [21–27], one finds different materials based on TiO_2. This oxide has been chosen as an anode due to the multiple advantages that it possesses [28–35]. Specifically, TiO_2 is nontoxic, chemically stable and it is a cost-effective material because of its abundance in the Earth's crust (0.62 %). Another important feature is that TiO_2 undergoes minor changes of volume during the charge-discharge process (< 4%), facilitating the design of mechanically stable electrodes. In fact, TiO_2 has been widely studied in the context of NIBs and the prospects of using it have been discussed for several morphologies, including nanoparticles [36–38], nanorods [39–41], nanofibers [42], nanotubes (NT) [43,44], etc. Specifically, capacity values between 70 and 250 $mA \cdot h \cdot g^{-1}$ have been reported for TiO_2 nanotube electrodes using rates from 10 C to 0.3 C and different types of conductive supports and additives. In the context of this study, the use of a reproducible electrode constituted only by amorphous TiO_2 nanotubes prepared by Ti anodization is relevant as it allows for a direct and reliable comparison.

We present here a comparative study on the electrochemical behavior of a TiO_2 nanotube electrode in a typical organic electrolyte such as 1 M $NaClO_4$/propylene carbonate and in $NaI \cdot 3.3NH_3$. Based on the results obtained, the potential advantages of liquid ammoniates as electrolytes in NIBs are also discussed.

2. Materials and methods

2.1. Preparation of TiO_2 nanotube electrodes

TiO_2 nanotube electrodes were prepared by anodization of a Ti foil (99.6%, Goodfellow) in a two-electrode electrochemical cell using gold foil as a cathode. Unless otherwise stated, the anodization was conducted at room temperature with a bias of 40 V for 1 h in a solution containing 80 % anhydrous ethylene glycol (99.8 %, Sigma Aldrich), 10 % dimethyl sulfoxide (99.9 %, Sigma Aldrich), 10 % deionized water and 0.15-0.35 M NH_4F (98 %, Sigma Aldrich). After anodization, the Ti foil was transferred to a vial containing ethanol and it was sonicated in a bath for 10 s. The electrode was dried at least for 4 hours in air prior to use. The amorphous NT electrodes were converted into anatase NT ones by submitting them to a thermal treatment at 500 °C for 1 hour in air.

2.2. Preparation of the organic electrolyte

The organic electrolyte was prepared by mixing 1.23 g $NaClO_4$ (98 %, Sigma Aldrich) in 10 mL of propylene carbonate anhydrous (99.7 %, Sigma Aldrich). The $NaClO_4$ was dried in a vacuum over at 120 °C overnight prior to use.

2.3. Preparation of the ammoniate electrolyte

The liquid ammoniate synthesis was carried out according to a procedure previously reported [45]. An excess of ammonia (Air Liquid) was condensed on NaI (Prolabo, dried at 120 °C in a vacuum oven for 3 days prior to use) at -50 °C. The resulting solution was colorless. The purification was performed by using solvated electrons: metallic sodium was added to the solution in large excess, immediately appearing the blue color characteristic of solvated electrons. These electrons react with impurities such as H_2O and O_2. Then the solution was left to slowly reach room temperature and it was centrifuged. Finally, the

electrolyte was stored in a glove box (H_2O < 0.5ppm, O_2 < 0.5 ppm). The composition was $NaI \cdot 3.3NH_3$ as found by weighing.

2.4. Materials characterization

The morphological characterization of TiO_2 nanotube electrodes was carried out by field emission scanning electron microscopy (FE-SEM) with a ZEIS Merlin VP Compact microscope. Transmission electron microscopy (TEM) was carried out by using a JEM-2010 (JEOL) microscope. The contact angle was determined by using a KSV CAM 101 optical contact angle meter.

2.5. Evaluation of the electrochemical behavior

Electrochemical characterization was performed by using either a standard three-electrode electrochemical cell or a two-electrode split cell, both assembled in a N_2-filled dry glove box (H_2O < 0.5 ppm, O_2 < 2 ppm) using TiO_2 NT on Ti foil as a working electrode and metallic sodium pieces as reference and counter electrodes. Either a 1 M $NaClO_4$ in PC solution or the ammoniate $NaI \cdot 3.3NH_3$ was used as the working electrolyte and two pieces of porous 435-µm-thick glass microfiber (Whatman 934-AH) were used as separators in the case of the two-electrode split cell. Cyclic voltammograms were recorded using a computer-controlled AUTOLAB potentiostat-galvanostat (PGSTAT30) in the range 0.5-2.6 V vs. Na^+/Na at ambient temperature (25 ± 2) ºC. The measurements were performed inside the glove box at scan rates of 50, 20, 10, 5 and 1 $mV \cdot s^{-1}$. The charge-discharge cycles were carried out in the potential window 0.5-2.6 V vs. Na^+/Na, using different C-rates: C/1 (0.1 mA), 2C (0.2 mA), 6C (0.5 mA) and 14C (1 mA, ~ 3000 $mA \cdot g^{-1}$). The C-values are calculated for the ammonaite. The geometric area of the electrodes was 1 cm^2 in all cases**.**

The potentiostat was equipped with an FRA module that enabled the obtainment of electrochemical impedance spectra (with an amplitude of 5 mV and in the frequency range

from 0.01 Hz to 100 kHz), which were acquired with the split cell. The experimental spectra were fitted with the software *EIS spectrum analyser*. It is a standalone program for analysis and simulation of impedance spectra.

3. Results and discussion

Fig. 1 shows cross-sectional and top view FE-SEM images of the TiO_2 electrodes. As observed, the electrodes are constituted by a dense array of nanotubes with 113±2 and 131±2 nm as average internal and external diameters, respectively, while their average height is of 3.5±0.1 µm. It is important to stress that, unless otherwise stated, no thermal annealing was applied after anodization.

One important source of inaccuracy in the calculation of electrode gravimetric capacities comes from uncertainties in the determination of the active material mass per electrode geometric area. This is particularly critical in the case of electrode materials prepared by anodization. The gravimetric capacity could be determined by weighing the NT film once mechanically detached from the substrate, but this may entail significant risks of underestimating the TiO_2 mass as some uncontrolled fragments of the material could remain attached to the substrate. Here the mass of active material is assessed through its volume via a detailed morphological analysis applied to a series of sample micrographs. A similar geometric approach has been considered previously for amorphous TiO_2 NT arrays [46]. An average active material mass density value of 0.34±0.04 $mg \cdot cm^{-2}$ can be thus calculated (see the Supplementary Material).

The TiO_2 electrode response was first examined by means of cyclic voltammograms obtained with a three-electrode cell with sodium counter and reference electrodes. Fig.

2a,b shows the stable voltammetric behavior at several scan rates for TiO_2 NT electrodes in contact with either 1 M $NaClO_4$/PC or $NaI \cdot 3.3NH_3$. Clear signs of sodium insertion are given by the specific currents and the shape of the voltammograms. This agrees with the first report on Na^+ ion insertion in TiO_2 NT electrodes [32]. Relatively large diameter NTs, as those forming the electrodes employed here, were required for sodium insertion.

The voltammetric behavior shown in Fig. 2 is more reversible in the case of the ammoniate, indicating that no transport limitations in the electrolyte are apparent in this case. As observed, in particular for the higher scan rates, the specific currents developed in the ammoniate are substantially larger than those in the organic electrolyte. Several factors could underlie the advantages of the ammoniate over the organic electrolyte. Certainly, the fact that both conductivity and sodium concentration are several times higher in the ammoniate avoids both an increase in electrolyte resistance and fast sodium depletion near the electrode material. In addition, the room-temperature ammoniate conductivity values reported in the literature vary from 85 to 140 $mS \cdot cm^{-1}$, while that of the 1 M $NaClO_4$/PC solution attains a value of 6.4 $mS \cdot cm^{-1}$ [12,20,47,48]. Furthermore, the NaI concentration in the ammoniate is as high as 7.6 M [19]. Some additional voltammetric experiments were carried out by using as an electrolyte 1 M sodium trifluoromethanesulfonate ($NaCF_3SO_3$) in dimethoxyethane (DME), showing lower performance than the 1 M $NaClO_4$/PC solution (see Fig. S3).

The limitation due to sodium depletion may be particularly severe for nanotubes with a high aspect ratio, in which the replenishment of sodium ions in the pore volume from the bulk solution may be slow, giving rise to transport problems. To further check this limitation, TiO_2 NT electrodes were prepared using different anodization times, leading to different NT lengths (see Fig. S4 in Supplementary data). Fig. 2c

shows the anodic charge recorded in positive-going voltammetric scans in the different electrolytes versus the NT length. For 1 M $NaClO_4$ in PC, the maximum charge is attained for 1 h anodization, while further increasing anodization times, and therefore NT lengths, is particularly beneficial for the ammoniate. In any case, the results in Fig. 2c indicate that the longer the tubes, the larger the benefits of using the ammoniate.

Fig. 3a,b shows charge/discharge curves obtained at two different current densities: Fig. 3a was acquired at 0.1 $mA \cdot cm^{-2}$ and Fig 3b at 1 $mA \cdot cm^{-2}$ for both organic (black curves) and inorganic (red curves) electrolytes. As commented above, the difference between both electrolytes becomes more profound for high charge/discharge rates. However, even in the case of the 0.1 $mA \cdot cm^{-2}$ both charge and discharge times are significantly larger for the ammoniate. The potential hysteresis in a charge/discharge curve indicates to what extent a certain electrochemical system will lead to batteries with a high energy efficiency, which can be evaluated as the ratio of the average voltages during discharge and charge. Such a potential hysteresis is larger in the case of the organic electrolyte, especially for the highest charge/discharge rate. This behavior results from the larger ohmic drop and transport limitations prevailing in the case of the organic electrolyte. Considering the data in Fig. 3b, the ratio of the average voltages during discharge and charge (energy efficiency) has values of 0.67 and 0.76 for the organic electrolyte and the ammoniate, respectively. Thus, a battery based on the ammoniate is expected to have a value of energy efficiency significantly larger than its organic counterparts.

On the other hand, Fig. 3c,d shows results about the effect of the charge/discharge rate on the gravimetric capacity of the TiO_2 NT electrodes together with information on their initial cyclability. For the organic electrolyte (Fig 3c) a stable electrochemical behavior is slowly reached, likely due to the formation of a deleterious SEI, which is

expected because of the organic carbonate decomposition [49]. In Fig. 3d a relatively fast increase in coulombic efficiency is observed for the $NaI \cdot 3.3NH_3$ electrolyte in the first 5-10 cycles, attaining finally a value close to 100 %. This is probably linked to an initial irreversible transformation of TiO_2 taking place during the first sodium insertion cycles, which is reflected in a permanent darkening of the TiO_2 NT electrode associated with the irreversible reduction of some Ti(IV) atoms. The permanent darkening is accompanied by the expected electrochemical modulation of coloration, which is more intense when a potential slightly above zero is applied (maximum sodium loading). (See Fig. S5 in the Supplementary data).

The gravimetric capacities are consistently higher for the ammoniate than for the organic electrolyte: at 0.1 $mA \cdot cm^{-2}$ by around a 10 % (from 160 $mAh \cdot g^{-1}_{TiO2}$ to 175 $mAh \cdot g^{-1}_{TiO2}$) and at 1 $mA \cdot cm^{-2}$ by around a 40 % (from 105 $mAh \cdot g^{-1}_{TiO2}$ to 145 $mAh \cdot g^{-1}_{TiO2}$). Finally, it is worth noting that comparable capacities have been reported by other authors for electrodes using conducting carbon and polymeric binder as additives, while in the case of the TiO_2 NT electrode reported here no such components are needed, which potentially makes its fabrication more feasible and low-cost. This also means that larger capacities calculated on the basis of the total electrode mass can be attained. To allow us to further assess electrode cyclability, Fig. 4 shows close to 400 charge/discharge cycles at 1 $mA \cdot cm^{-2}$ for both the organic and the ammoniate electrolytes, confirming the tendencies shown in Fig. 3c,d for the initial stability of the electrode and interfacial regions.

The fact that the difference between both electrolytes is clearer for high charge/discharge rates points anew to the importance of the increase in both conductivity and, particularly, sodium concentration of the ammoniate with respect to the organic electrolyte. A simple calculation is useful to realize to what extent the high

sodium concentration may be critical in the case of highly porous electrodes. Assuming the nanotube geometric parameters given above and considering that full sodium intercalation under the conditions employed here (discharge performed at $0.1 mA \cdot cm^{-2}$) leads to a final stoichiometry $Na_{0.57}TiO_2$, a total of $3.07 \cdot 10^8$ Na^+ ions would need to intercalate to fully sodiate one nanotube. On the other hand, based on the sodium concentration in the ammoniate, the inner pore volume of one NT is calculated to accommodate $1.6 \cdot 10^8$ Na^+ ions assuming that the Na^+ concentration is homogeneous throughout the entire tube length. This means that the electrolyte within the nanotube before Na^+ intercalation contains 52 % of the Na^+ ions needed for full intercalation. This is in stark contrast with the situation in 1 M electrolytes, for which the above-mentioned percent is only of a 6.8 %. This clearly imposes sodium transport limitations particular at high C rates in the case of the organic electrolyte that would be absent for the ammoniate.

A factor that should also be considered for explaining the gravimetric capacity results is the ability of the electrolytes to wet the TiO_2 surface, which could be problematic in the case of highly concentrated solutions. High wettability should favor both maximum interfacial area and full utilization of the active material. In principle, the ammoniate electrolyte, despite its very high sodium concentration, should efficiently wet the surface of the TiO_2 NTs as the ammonia molecules can favorably interact with both titanium and oxygen surface atoms via the unpaired electrons and through the formation of hydrogen bridge bonds, respectively. Contact angle measurements were performed for the ammoniate on TiO_2 showing values similar (or even smaller) than those corresponding to a $NaClO_4$ saturated solution in PC, even when the sodium molar concentration in the latter is barely one third that in the ammoniate (see Table S1 in the Supplementary data).

In addition, with the aim to further evaluate the superior electrochemical performance of $NaI \cdot 3.3NH_3$ over 1 M $NaClO_4$/PC in NIBs, a comparative study was carried out using electrodes based on TiO_2NT crystallized into anatase or reduced graphene oxide (rGO) as anode materials. The TiO_2 nanotubes were submitted to a thermal treatment at 500 ºC for 1h in air, leading to their transformation into anatase. Cyclic voltammograms were acquired for both electrolytes (Fig. 5). In the case of the ammoniate, the pseudocapacitive processes associated to sodium insertion are observed at lower potentials, closer to the sodium plating potential, which is advantageous to obtain higher voltages in NIBs, although it could also lead to undesired Na plating. This behavior results from the change in the electronic structure of TiO_2 triggered by crystallization. In fact, for the insertion of sodium to occur in anatase, the potential corresponding to the surface state distribution existing just below the conduction band edge must be attained [50]. In the case of the amorphous material, this tail of surface and defect states is expected to extend significantly more into the band gap of the material. In addition, the density of such defect states would also increase. These two factors favor the use of amorphous materials for sodium insertion batteries and hybrid supercapacitors. In addition, the higher flexibility of the amorphous structure would also allow for a more straightforward accommodation of the changes in volume concomitant with insertion. In contrast, when the TiO_2NT anatase electrode was characterized in the organic medium (1 M $NaClO_4$/PC, Fig 5 black curve), the sodium insertion process was observed to be less reversible, desodiation taking place at more positive potentials. This strengthens the limitations associated to the use of organic electrolytes and crystalline structures.

Finally, a similar comparative study between inorganic and organic electrolytes was also performed using a carbon-based electrode such as reduced graphene oxide (rGO).

The electrochemical behavior of the electrode was again observed to be dramatically superior in the $NaI \cdot 3.3NH_3$, obtaining CVs comparable to those of a related lithium system [53] (more details can be found in the SM, Fig. S6).

To gain further understanding on the factors determining the ammoniate superior performance, cells containing both electrolytes were comparatively studied by means of EIS. The corresponding Nyquist plots are shown in Fig. 6. For the organic electrolyte (Fig. 6a), a semicircle is observed at high frequencies, while at low frequencies straight lines with a slope higher than one appear regardless of the potential applied. The semicircle can be associated with a resistive-capacitive contribution with its diameter corresponding to the value of the charge transfer resistance. The linear region points to the existence of diffusion limitation for the sodium ion transport in the TiO_2. The slope above unity indicates that diffusion within a nanotube cannot be considered as occurring in a semi-infinite planar domain as it is bounded by the space in the active material [51]. As expected, analogous linear regions at low frequencies appear with the ammoniate (Fig. 6b). For both electrolytes, such a linear part slightly depends on potential, which can be understood based on both the strong dependence on potential of the amount of intercalated sodium and the associated changes in the solid structure. Importantly, in the case of the ammoniate, the semicircles at high frequencies are barely distinguishable because of their small radii.

With the aim to do a semi-quantitave comparison between the EIS spectrum obtained for both systems (based on organic and inorganic electrolytes), a simplified equivalent electric circuit was performed using the software *EIS Spectrum Analyser*, Fig. 7a. The circuit contains four elements: R_e, CPE, R_{ct} and W, representing the electrolyte resistance, a constant phase element, the charge transfer resistance and a

Warburg element, respectively. The value for R_e can be estimated from the intersection of the spectrum with the real impedance axis in the high frequency limit. The CPE is related to the double-layer capacitance of a real system [52–54]. The impedance associated with the CPE is given by eq. (1) [55].

$$Z_{CPE} = Z_0(i\omega)^{-n} \qquad \text{eq. (1)}$$

where Z_0 and n are independent of frequency. If n equals 0, then the CPE is equivalent to a resistance with $R = Z_0$. If n is 1, the CPE converts into a capacitor. In general, when $n > 0.8$, the CPE can be considered as a capacitor. On the other hand, R_{ct} can be estimated as the radius of the semicircle. Finally, the Warburg element derives in this case from the diffusion limitation associated to the transport of sodium ion within the TiO_2 walls [56].

Fig. 7b contains the Nyquist plot with the EIS experimental points (red symbols) obtained for the organic electrolyte at a potential 1.81 V. In addition, the fitted simulated spectrum is also shown (black symbols). As observed, the fit is excellent in the high frequency region semicircle, while a significant deviation is observed in the linear region at low frequency. As commented above, this apparent discrepancy results from the fact that sodium diffusion is confined to the TiO_2 wall thickness whereas the Warburg element corresponds to diffusion limitations in a semi-infinite domain. Fig. 7c contains the corresponding data for the ammoniate: red symbols refer to experimental data and blue symbols refer to simulated spectrum using above-named software. As in the organic electrolyte case, there is a discrepancy between the experimental and simulated spectra for the low frequency region. In addition, the high frequency semicircle in this case is poorly defined.

Even though there is a deviation between the fitted or simulated curves with respect to the experimental curves for both organic and inorganic electrolytes, a semi-

quantitative comparison can be done between the values of the parameters of the electric circuit. Table 1 contains the fitted values for the elements of the circuit for both electrolytes. As the simple circuit proposed does not lead to a good fit, the values resulting for the element should be considered only at a semi-quantitative level. Nevertheless, the values of the parameters of the electric circuit can be also estimated from the experimental curve considering the descriptions done in the above paragraph. For both electrolytes, the value of n in eq. (1) could be made equal to one, without observing a deleterious effect on the fit. As expected, R_e is larger in the organic electrolyte due to the fact that its specific conductivity is significantly lower than that of the inorganic electrolyte. On the other hand, the value obtained for the CPE element (capacitance) in the ammoniate is over two orders of magnitude higher than that of the organic electrolyte. This can be attributed to the formation of a SEI in the case of the organic electrolyte. The SEI capacitance is expected to be inversely proportional to the thickness of the solid electrolyte film. In principle, it should be much smaller than a chemical capacitance or that associated to the Helmholtz layer. Such a SEI would be absent in the case of the ammoniate as, in this case, no evidence for the formation of a SEI has been found. This would explain the much larger value of the capacitance in the case of the ammoniate. Finally, a critical difference between both electrolytes is found in the values of R_{ct}. As observed, the R_{ct} value for the inorganic electrolyte is extremely low, which explains that the semicircle in the Nyquist plot representation is barely discernible. In contrast, the R_{ct} in the organic electrolyte is 2-3 orders of magnitude larger, which derives from the lower sodium concentration together with a less favorable interface configuration and speciation in the electrolyte than for the ammoniate. In particular, the TiO_2/electrolyte would be free of the SEI, thus facilitating the charge transfer between solid and solution.

4. Conclusions

In summary, the prospects of using the ammoniate of sodium iodide as an electrolyte in NIBs have been illustrated by comparing the behavior of amorphous TiO_2 NT electrodes with conventional sodium electrolytes such as that constituted by 1 M $NaClO_4$ in PC. In general, larger gravimetric capacities are obtained in $NaI \cdot 3.3NH_3$. Even at a specific current as high as 3000 $mA \cdot g^{-1}$, a capacity value of 150 $mA \cdot h \cdot g^{1}$ can be obtained for the ammoniate. Importantly, the characteristics of the liquid ammoniate make it suitable for applications in the field of batteries and supercapacitors as it possesses a very high concentration of sodium ions (1 Na^+ ion per 3.3 NH_3 molecules), a rather high ionic conductivity (around 100 $mS \cdot cm^{-1}$) and ability to wet different types of surfaces. One of the most important properties of the ammoniate is that it does not tend to form SEIs, which results in much higher values for the electrochemical capacitance and much smaller charge transfer resistances. In fact, the liquid ammoniates may be considered as a special type of ionic liquid in which the ionic compound would be an ammonia solvate. Apart from the favorable physical characteristics of the ammoniates and being characterized by a very low charge transfer resistance for TiO_2 NT electrodes, its relative environmental benignity, low flammability and cost effectiveness make advisable to further explore their applicability in the field of sodium-based batteries. Specifically, a crude economic estimate reveals that the cost of the ammoniate can be just one third of that for typical organic electrolytes. It is expected that the advantages shown by the ammoniate in the case of TiO_2 are also kept for other electrode materials as shown here in the case of anatase NTs and, in a preliminary way, for electrodes based on reduced graphene oxide. Further studies along these lines are under way in our laboratory. Specifically, we are focusing on the development of new ammoniates with low volatility, the use of other TiO_2 nanostructures and of new insertion materials.

Acknowledgment

Funding: this work was partly supported by the Ministry of Science, Innovation and Universities through projects MAT2015-71727-R and RTI2018-102061-B-I00 (FONDOS FEDER).

Appendix A. Supplementary data

Table 1. Fitted values for the different elements in the circuit shown in Fig. 7a and b for both the ammoniate and the organic electrolyte (1 M $NaClO_4$ in propylene carbonate). Electrode projected area of 1 cm^2.

Element of the equivalent circuit	**Fitted values**	
	$NaI \cdot 3.3NH_3$	1 M $NaClO_4$/PC
Re / Ω	3.9	7.6
CPE / F	$7.7 \cdot 10^{-5}$	$5.2 \cdot 10^{-7}$
R_{tc} / Ω	0.05	19.4

Figure captions

Fig. 1. (a) Top-view FE-SEM image corresponding to a TiO_2 nanotube array. The inset shows a detail of the nanostructure at a higher magnification. (b) Cross-sectional FE-SEM image of a TiO_2 array.

Fig. 2. Voltammetric behavior of the TiO_2 nanotube electrodes (expressed in terms of specific current) for both 1 M $NaClO_4$/PC (a) and $NaI \cdot 3.3NH_3$ (b) at different scan rates. (c) Charge integrated in the positive-going voltammetric scans (10 $mV \cdot s^{-1}$ between 0.5 V and 2.6 V) measured in different electrolytes for amorphous TiO_2 NT electrodes as a function of the anodization time: Blue squares: $NaI \cdot 3.3NH_3$; Black circles; 1 M $NaClO_4$ in PC; Red triangles: $NaCF_3SO_3$ in DME.

Fig. 3. Charge/discharge curves at (a) 0.1 $mA \cdot cm^{-2}$ and (b) 1 $mA \cdot cm^{-2}$ for the TiO_2 NT electrodes in $NaI \cdot 3.3NH_3$ (red line) and 1 M $NaClO_4$/PC (black line). Coulombic efficiency and gravimetric capacity as a function of the number of cycles at different charge/discharge rates for TiO_2 NT electrodes in contact with (c) 1 M $NaClO_4$ in PC and (d) $NaI \cdot 3.3NH_3$.

Fig. 4. Coulombic efficiency and gravimetric capacity as a function of the number of cycles in (a) 1 M $NaClO_4$/PC and (b) $NaI \cdot 3.3NH_3$ for TiO_2 NT electrode at 1 $mA \cdot cm^{-2}$ rate.

Fig. 5. Cyclic voltammograms obtained for anatase nanotube electrodes prepared by thermal annealing of amorphous TiO_2 electrodes synthesized by anodization in contact with either 1 M $NaClO_4$ in propylene carbonate or $NaI \cdot 3NH_3$. Scan rate: 10 $mV \cdot s^{-1}$.

Fig. 6. Impedance spectra **(**Nyquist plots) for amorphous TiO_2 electrodes for both 1 M $NaClO_4$/PC (a) and $NaI \cdot 3.3NH_3$ (b) at different applied potentials. The inset in panel b shows a detail of the plots. The frequencies of some points are indicated by means of labels.

Fig. 7. (a) Equivalent electric circuit for the interpretation of electrochemical impedance spectroscopy for both organic and inorganic system. (b,c) Experimental Nyquist plots (red symbols) together with the fitted spectra (black and blue symbols for 1 M $NaClO_4$/PC and $NaI \cdot 3.3NH_3$, respectively).

Data availability

The raw/processed data required to reproduce these findings cannot be shared at this time due to technical or time limitations.

References

[1] B. Dunn, H. Kamath, J.M. Tarascon, Electrical Energy Storage for the Grid: A Battery of Choices, Science (80-.). 334 (2011) 928–935. doi:10.1126/science.1212741.

[2] S.P.S. Badwal, S.S. Giddey, C. Munnings, A.I. Bhatt, Hollenkamp, A.F., Emerging electrochemical energy conversion and storage technologies., Front. Chem. 2 (2014) 79. doi:10.3389/fchem.2014.00079.

[3] M.S. Whittingham, History, Evolution, and Future Status of Energy Storage, Proc. IEEE. 100 (2012) 1518–1534. doi:10.1109/JPROC.2012.2190170.

[4] M. Armand, J.M. Tarascon, Building better batteries, Nature. 451 (2008) 652–657. doi:10.1038/451652a.

[5] S. M. Kimball, USGS Mineral Commodities Summaries, 2016. doi:10.3133/70140094.

[6] B. Scrosati, J. Garche, Lithium batteries: Status, prospects and future, J. Power Sources. 195 (2010) 2419–2430. doi:10.1016/j.jpowsour.2009.11.048.

[7] G. Ceder, Y.M. Chiang, D.R. Sadoway, M.K. Aydinol, Y.I. Jang, B. Huang, Identification of cathode materials for lithium batteries guided by first-principles calculations, Nature. 392 (1998) 694–696. doi:10.1038/33647.

[8] N. Yabuuchi, K. Kubota, M. Dahbi, S. Komaba, Research development on sodium-ion batteries., Chem. Rev. 114 (2014) 11636–11682. doi:10.1021/cr500192f.

[9] D. Wu, X. Li, B. Xu, N. Twu, L. Liu, G. Ceder, NaTiO2: a layered anode material for sodium-ion batteries, Energy Environ. Sci. 8 (2015) 195–202. doi:10.1039/C4EE03045A.

[10] M. Sawicki, L.L. Shaw, Advances and challenges of sodium ion batteries as post lithium ion batteries, RSC Adv. 5 (2015) 53129–53154. doi:10.1039/C5RA08321D.

[11] V.D. D. Kundu, E. Talaie, L.F. Nazar, The emerging chemistry of Sodium Ion Batteries for Electrochemical Energy Storage, Angew. Chem. Int. Ed. 54 (2015) 3431–3448. doi:.org/10.1002/anie.201410376.

[12] A. Ponrouch, D. Monti, A. Boschin, B. Steen, P. Johansson, M.R. Palacín, Non-aqueous electrolytes for sodium-ion batteries, J. Mater. Chem. A. 3 (2015) 22–42.

doi:10.1039/C4TA04428B.

[13] C.Y. Chen, T. Kiko, T. Hosokawa, K. Matsumoto, T. Nohira, R. Hagiwara, Ionic liquid electrolytes with high sodium ion fraction for high-rate and long-life sodium secondary batteries, J. Power Sources. 332 (2016) 51–59. doi:10.1016/j.jpowsour.2016.09.099.

[14] G.A. Giffin, Ionic Liquid-based Electrolytes for "Beyond Lithium" Battery Technologies, J. Mater. Chem. A. 4 (2016) 13378–13389. doi:10.1039/C6TA05260F.

[15] A. Ponrouch, E. Marchante, M. Courty, J.-M. Tarascon, M.R. Palacín, In search of an optimized electrolyte for Na-ion batteries, Energy Environ. Sci. 5 (2012) 8572–8583. doi:10.1039/c2ee22258b.

[16] L. Otaegui, E. Goikolea, F. Aguesse, M. Armand, T. Rojo, G. Singh, Effect of the electrolytic solvent and temperature on aluminium current collector stability: A case of sodium-ion battery cathode, J. Power Sources. 297 (2015) 168–173. doi:10.1016/j.jpowsour.2015.07.084.

[17] J.B. Goodenough, Y. Kim, Challenges for rechargeable Li batteries, Chem. Mater. 22 (2010) 587–603. doi:10.1021/cm901452z.

[18] F. Colò, F. Bella, J.R. Nair, M. Destro, C. Gerbaldi, Cellulose-based novel hybrid polymer electrolytes for green and efficient Na-ion batteries, Electrochim. Acta. 174 (2015) 185–190. doi:10.1016/j.electacta.2015.05.178.

[19] D. Ruiz-Martínez, A. Kovacs, R. Gómez, Development of novel inorganic electrolytes for room temperature rechargeable sodium metal batteries, Energy Environ. Sci. 10 (2017) 1936–1941. doi:10.1039/C7EE01735A.

[20] J. Badoz-Lambling, M. Bardin, C. Bernard, B. Fahys, M. Herlem, A. Thiebault., G. Robert, new battery electrolytes for low and high temperatures: Liquid and solid ammoniates for high energy batteries, J. Electrochem. Soc. 135 (1988) 587–591. doi:10.1149/1.2095662.

[21] M. Zhou, Y. Xu, J. Xiang, C. Wang, L. Liang, L. Wen, Y. Fang, Y. Mi, Y. Lei, Understanding the Orderliness of Atomic Arrangement toward Enhanced Sodium Storage, Adv. Energy Mater. 6 (2016) 1600448. doi:10.1002/aenm.201600448.

[22] D. Yan, L. Pan, A new sodium storage mechanism of TiO_2 for sodium ion batteries, Inorg. Chem. Front. 3 (2016) 464–468. doi:10.1039/C5QI00226E.

[23] S. Li, L. Xie, H. Hou, H. Liao, Z. Huang, X. Qiu, X. Ji, Alternating voltage induced ordered anatase TiO2 nanopores: An electrochemical investigation of sodium storage, J. Power Sources. 336 (2016) 196–202. doi:10.1016/j.jpowsour.2016.10.072.

[24] Y. Li, Y. Lu, C. Zhao, Y.-S. Hu, M.-M. Titirici, H. Li, X. Huang, L. Chen, Recent advances of electrode materials for low-cost sodium-ion batteries towards practical application for grid energy storage, Energy Storage Mater. 7 (2017) 130–151. doi:10.1016/j.ensm.2017.01.002.

[25] D. Li, L. Zhang, H. Chen, J. Wang, L.-X. Ding, S. Wang, P.J. Ashman, H. Wang, Graphene-based nitrogen-doped carbon sandwich nanosheets: a new capacitive process controlled anode material for high-performance sodium-ion batteries, J. Mater. Chem. A. 4 (2016) 8630–8635. doi:10.1039/C6TA02139E.

[26] D. Yan, C. Yu, D. Li, X. Zhang, J. Li, T. Lu, L. Pan, Improved sodium-ion storage performance of TiO_2 nanotubes by Ni^{2+} doping, J. Mater. Chem. A. 4 (2016) 11077–11085. doi:10.1039/C6TA04906K.

[27] J. Lee, J.K. Lee, K.Y. Chung, H.G. Jung, H. Kim, J. Mun, W. Choi, Electrochemical Investigations on TiO_2-B Nanowires as a Promising High Capacity Anode for Sodium-ion Batteries, Electrochim. Acta. 200 (2016) 21–28. doi:10.1016/j.electacta.2016.03.110.

[28] C. Bommier, D. Leonard, Z. Jian, W.F. Stickle, P.A. Greaney, X. Ji, New Paradigms on the Nature of Solid Electrolyte Interphase Formation and Capacity Fading of Hard Carbon Anodes in Na-Ion Batteries, Adv. Mater. Interfaces. 3 (2016) 1600449. doi:10.1002/admi.201600449.

[29] Y. Xu, M. Zhou, L. Wen, C. Wang, H. Zhao, Y. Mi, L. Liang, Q. Fu, M. Wu, Y. Lei, Highly Ordered Three-Dimensional Ni-TiO_2 Nanoarrays as Sodium Ion Battery Anodes, Chem. Mater. 27 (2015) 4274–4280. doi:10.1021/acs.chemmater.5b00633.

[30] X. Yang, C. Wang, Y. Yang, Y. Zhang, X. Jia, J. Chen, X. Ji, Anatase TiO_2 nanocubes for fast and durable sodium ion battery anodes, J. Mater. Chem. A. 3 (2015) 8800–8807. doi:10.1039/C5TA00614G.

[31] Y. Yeo, J.-W. Jung, K. Park, I.-D. Kim, Graphene-Wrapped Anatase TiO_2 Nanofibers as High-Rate and Long-Cycle-Life Anode Material for Sodium Ion Batteries, Sci. Rep. 5 (2015) 13862. doi:10.1038/srep13862.

[32] H. Xiong, M.D. Slater, M. Balasubramanian, C.S. Johnson, T. Rajh, Amorphous TiO_2 Nanotube anode for rechargeable sodium ion batteries, J. Phys. Chem. Lett. 2 (2011) 2560–2565. doi:10.1021/jz2012066.

[33] I.B.I. J. Y. Hwanga, S. T. Myungb, J. H. Lee, A. Abouimrane, Y.K. Sun, Ultrafast sodium storage in anatase TiO_2 nanoparticles embedded on carbon nanotubes, Nano Energy. 16 (2015) 218–226. doi:.org/10.1016/j.nanoen.2015.06.017.

[34] J. Liang, Z. Wang, Z. Li, X. Wang, K. Yu, Fabrication of Nanostructured TiO_2 Using a Solvothermal Reaction for Lithium-ion Batteries, Nanomater. Nanotechnol. 6 (2016) doi: 10.5772/62420. doi:10.5772/62420.

[35] I.H.O. J.H. Kim, W. Choi, H.G. Jung, S.H. Og, K.Y. Chung, W. I. Cho, I.W. Nah, Anatase TiO_2-reduced graphene oxide nanoestructures with high-rate sodium storage performance, J. Alloy. Compd. 690 (2017) 390–396. doi:.org/1010/j.jallcom.2016.08.140.

[36] M.N. Tahir, B. Oschmann, D. Buchholz, X. Dou, I. Lieberwirth, M. Panthöfer, W. Tremel, R. Zentel, S. Passerini, Extraordinary Performance of Carbon-Coated Anatase TiO2 as Sodium-Ion Anode, Adv. Energy Mater. 6 (2016) 1501489. doi:10.1002/aenm.201501489.

[37] H.A. Cha, H.M. Jeong, J.K. Kang, Nitrogen-doped open pore channeled graphene facilitating electrochemical performance of TiO_2 nanoparticles as an anode material for sodium ion batteries, J. Mater. Chem. A. 2 (2014) 5182–5186. doi:10.1039/c4ta00041b.

[38] Y. Ge, H. Jiang, J. Zhu, Y. Lu, C. Chen, Y. Hu, Y. Qiu, X. Zhang, High cyclability of carbon-coated TiO_2 nanoparticles as anode for sodium-ion batteries, Electrochim. Acta. 157 (2015) 142–148. doi:10.1016/j.electacta.2015.01.086.

[39] Y.C. Yang, X.B. Ji, M.J. Jing, H.S. Hou, Y.R. Zhu, L.B. Fang, X.M. Yang, Q.Y. Chen, C.E. Banks, Carbon dots supported upon N-doped TiO_2 nanorods applied into sodium and lithium ion batteries, J. Mater. Chem. A. 3 (2015) 5648–5655. doi:10.1039/c4ta05611f.

[40] X. Gu, L. Li, Y. Wang, P. Dai, H. Wang, X. Zhao, Hierarchical tubular structures constructed from rutile TiO2 nanorods with superior sodium storage properties, Electrochim. Acta. 211 (2016) 77–82. doi:10.1016/j.electacta.2016.06.029.

[41] Q. Zhou, L. Liu, J. Tan, Z. Yan, Z. Huang, X. Wang, Synthesis of lithium titanate nanorods as anode materials for lithium and sodium ion batteries with superior electrochemical performance, J. Power Sources. 283 (2015) 243–250. doi:10.1016/j.jpowsour.2015.02.061.

[42] K.N. Jung, J.Y. Seong, S.S. Kim, G.J. Lee, J.W. Lee, One-dimensional nanofiber architecture of an anatase TiO_2 –carbon composite with improved sodium storage performance, RSC Adv. 5 (2015) 106252–106257. doi:10.1039/C5RA14655K.

[43] D. Ya, C. Yu, Y. Bai, W. Zhang, T. Chen, B. Hu, Z. Sun, L. Pan, Sn-doped TiO_2 nanotubes as superior anode materials for sodium ion batteries, Chem. Commun. 51

(2015) 8261–8264.

[44] Gonzalez J.R., R. Alcantara, F. Nacimiento, G.F. Ortiz, T.J. L., Self-organized, anatase, double-walled nanotubes prepared by anodization under voltage ramp as negative electrode for aqueous sodium-ion batteries, J. Electrochem. Soc. 162 (2015) A3007–A3012.

[45] A.M. Goncalves, P. Tran-Van, G. Herlem, E. Kwa, B. Fahys, M. Herlem, New Potential Candidates for Redox Battery Using Liquid Ammoniates: Na^+/Na and Ag+/Ag, Port. Electrochim. Acta. 26 (2006) 117–127.

[46] Q.L. Wu, J. Li, R.D. Deshpande, N. Subramanian, S.E. Rankin, F. Yang, Y.T. Cheng, Aligned TiO_2 nanotube arrays as durable lithium-ion battery negative electrodes, J. Phys. Chem. C. 116 (2012) 18669–18677. doi:10.1021/jp3072266.

[47] M. Herlem, M. Székely, E. Sutter, C. Mathieu, A.M. Gonçalves, E. Caillot, G. Herlem, B. Fahys, Liquid ammoniates: Nonaqueous electrolytes for electrochromism, Electrochim. Acta. 46 (2001) 2967–2973. doi:10.1016/S0013-4686(01)00514-X.

[48] M. Egashira, T. Tanaka, N. Yoshimoto, M. Morita, Influence of Ionic Liquid Species in Non-Aqueous Electrolyte on Sodium Insertion into hard Carbon, Electrochemistry. 80 (2012) 755–758. doi:.org/10.5796/electrochemistry.80.755.

[49] L. Wu, D. Bresser, D. Buchholz, S. Passerini, Nanocristalline TiO_2(B) as Anode Material for Sodium-ion Batteries, J. Electrochem. Soc. 162 (2015) A3052–A3058. doi:10.1149/2.0091502jes.

[50] M. Jankulovska, T. Berger, S.S. Wong, R. Gómez, T. Lana-Villarreal, Trap states in TiO_2 films made of nanowires, nanotubes or nanoparticles: An electrochemical study, ChemPhysChem. 13 (2012) 3008–3017. doi:10.1002/cphc.201200072.

[51] J. Song, M.Z. Bazant, Effects of Nanoparticle Geometry and Size Distribution on Diffusion Impedance of Battery Electrodes, J. Electrochem. Soc. 160 (2013) A15–A24. doi:10.1149/2.023301jes.

[52] D. Yan, C. Yu, X. Zhang, J. Li, J. Li, T. Lu, L. Pan, Enhanced electrochemical performances of anatase TiO_2 nanotubes by synergetic doping of Ni and N for sodium-ion batteries, Electrochim. Acta. 254 (2017) 130–139. doi:10.1016/j.electacta.2017.09.120.

[53] D. Yan, C. Yu, D. Li, X. Zhang, J. Li, T. Lu, L. Pan, Improved sodium-ion storage performance of TiO_2 nanotubes by Ni2+doping, J. Mater. Chem. A. 4 (2016) 11077–11085. doi:10.1039/c6ta04906k.

[54] D. Yan, X. Xu, T. Lu, B. Hu, D.H.C. Chua, L. Pan, Reduced graphene oxide/carbon

nanotubes sponge: A new high capacity and long life anode material for sodium-ion batteries, J. Power Sources. 316 (2016) 132–138. doi:10.1016/j.jpowsour.2016.03.050.

[55] M.I. Díez García, R. Gómez, Investigating Water Splitting with $CaFe_2O_4$ Photocathodes by Electrochemical Impedance Spectroscopy, 2016. doi:10.1021/acsami.6b07465.

[56] J. Bisquert, G. Garcia-Belmonte, P. Bueno, E. Longo, L.O.S. Bulhões, Impedance of constant phase element (CPE)-blocked diffusion in film electrodes, J. Electroanal. Chem. 452 (1998) 229–234. doi:10.1016/S0022-0728(98)00115-6.

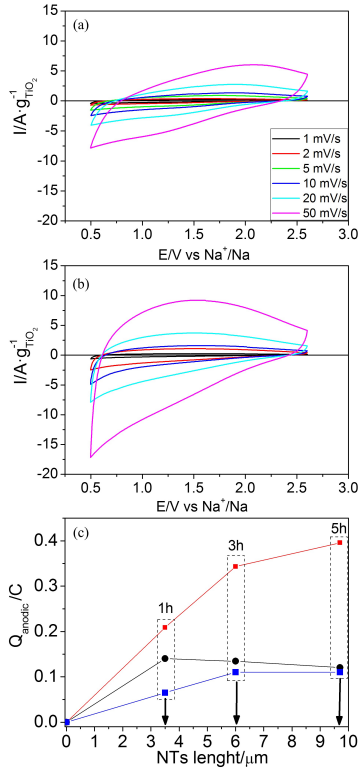

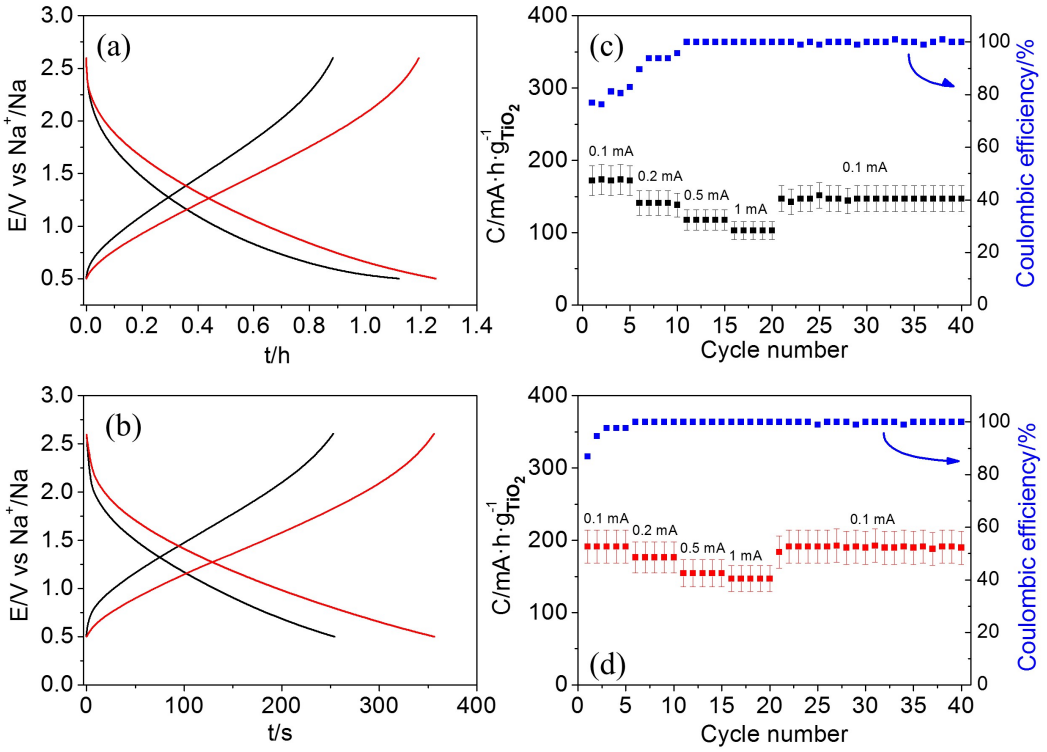
(a)
E/V vs Na+/Na
t/h
(b)
E/V vs Na+/Na
t/s
(c)
C/mA·h·gTiO2-1
Coulombic efficiency/%
Cycle number
0.1 mA
0.2 mA
0.5 mA
1 mA
0.1 mA
(d)
C/mA·h·gTiO2-1
Coulombic efficiency/%
Cycle number
0.1 mA
0.2 mA
0.5 mA
1 mA
0.1 mA

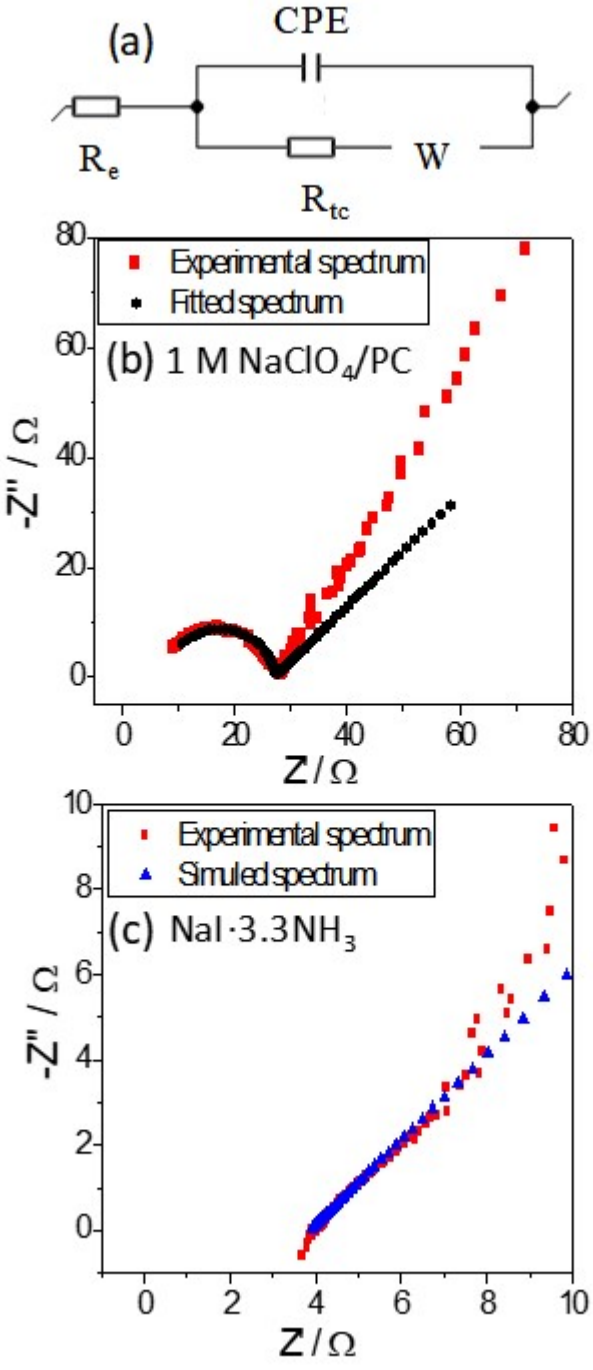
(a)
CPE
R_e
W
R_{tc}
Experimental spectrum
Fitted spectrum
(b) 1 M $NaClO_4$/PC
-Z'' / Ω
Z / Ω
Experimental spectrum
Simuled spectrum
(c) NaI·3.3NH_3
-Z'' / Ω
Z / Ω

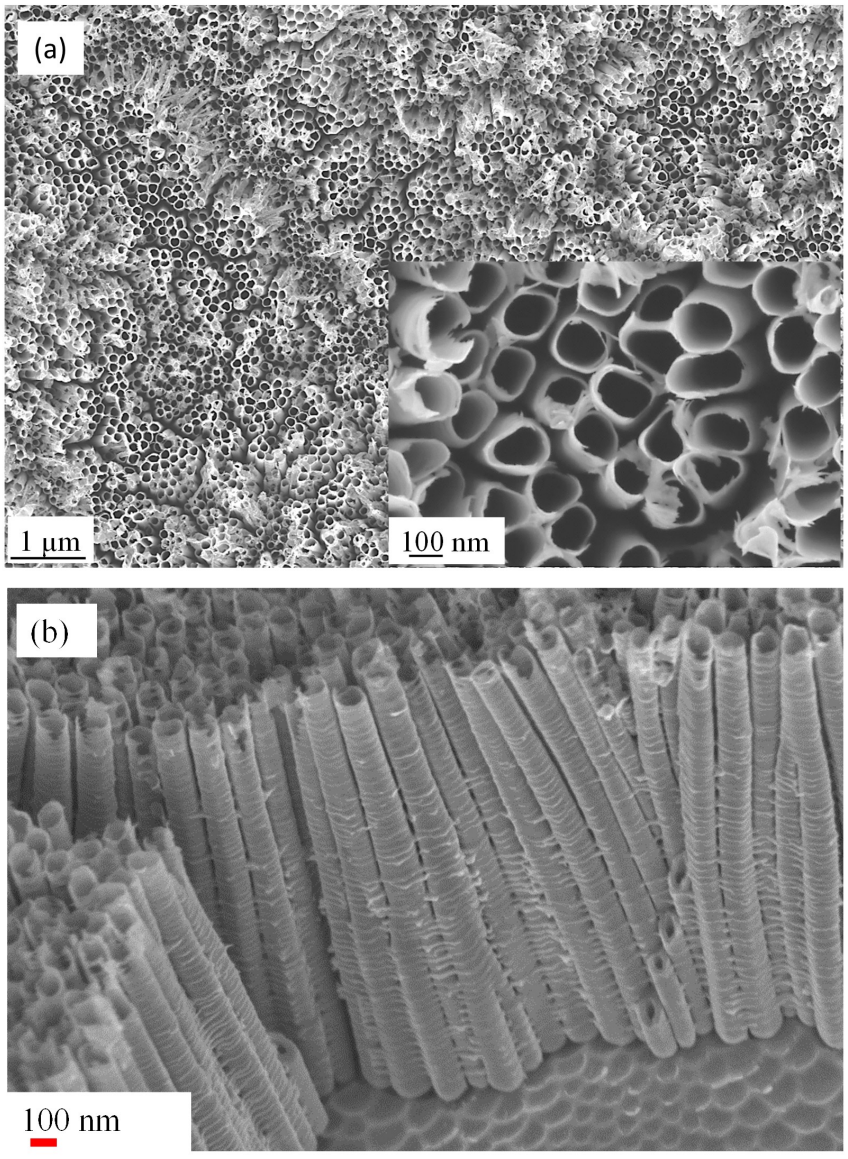

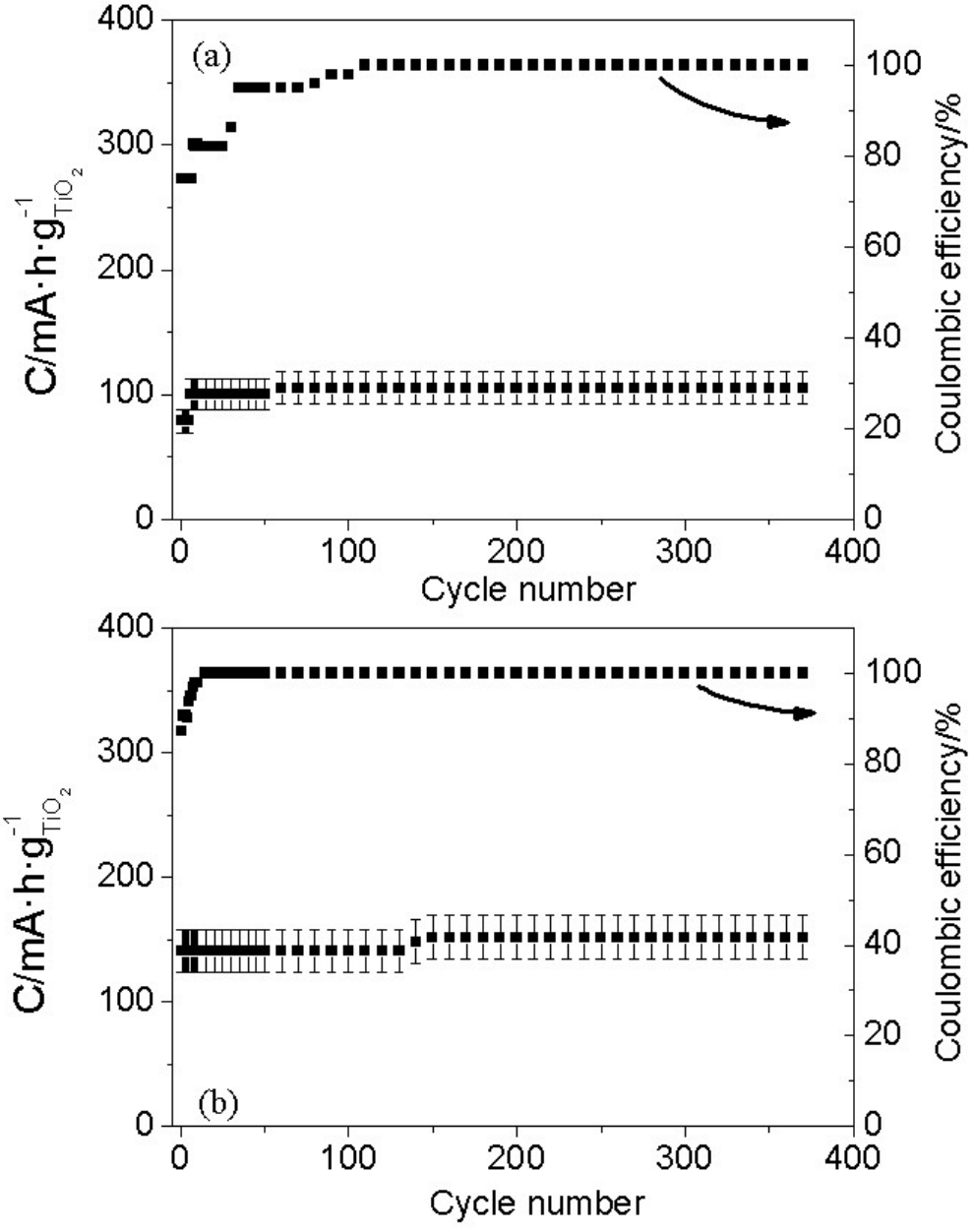
(a)
(b)
C/mA·h·g$^{-1}_{TiO_2}$
Coulombic efficiency/%
Cycle number
0
100
200
300
400
0
20
40
60
80
100

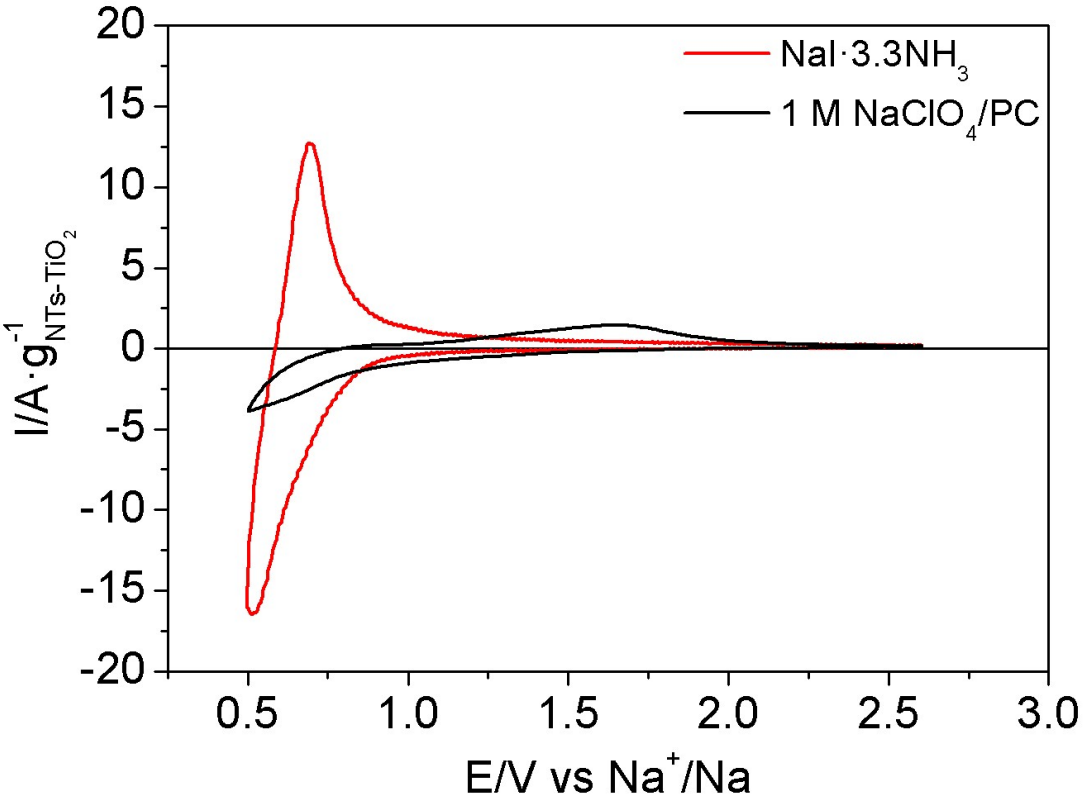
NaI·3.3NH3
1 M NaClO4/PC
I/A·g-1NTs-TiO2
E/V vs Na+/Na
20
15
10
5
0
-5
-10
-15
-20
0.5
1.0
1.5
2.0
2.5
3.0

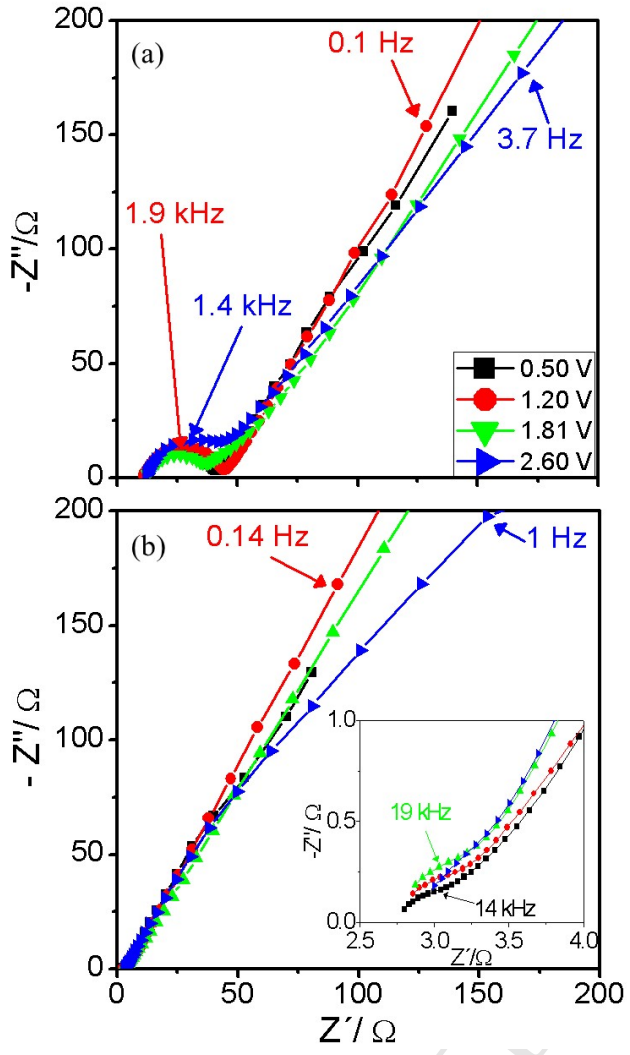

Supplementary Material

The Liquid Ammoniate of Sodium Iodide as an Alternative Electrolyte for Sodium Ion Batteries: the Case of Titanium Dioxide Nanotube Electrodes

CONTENT

Estimation of the electrode TiO_2 active mass

The estimation has been performed on the basis of geometric calculations by assimilating the shape of a NT to that of a relatively simple 3D geometric element. With such a purpose TEM images of complete NTs were collected. Figure S1 corresponds to one representative image. As observed, the thickness of the NT wall steadily decreases with the distance to the bottom of the tubes. Therefore, a nanotube is considered to be a tube with a pore with a circular cross section of variable diameter. It is also relevant that the tubes have a relatively thick base. Scheme S1 shows the idealized shape of one nanotube.

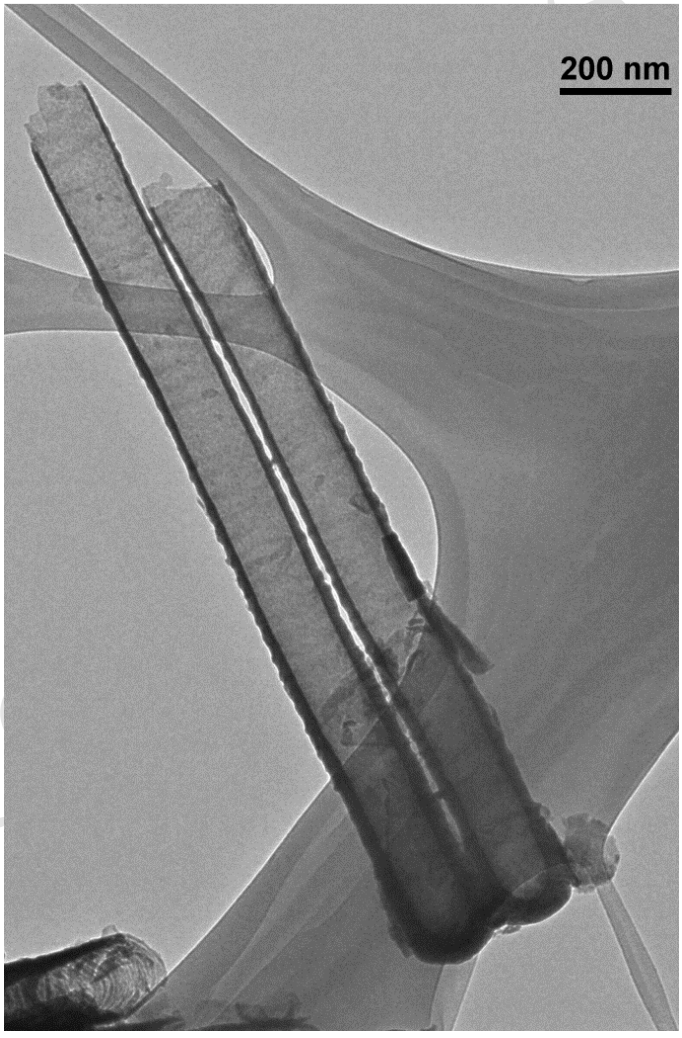

Figure S1. Transmission Electron Microscopy image of a couple of NTs detached from the TiO_2 NT film.

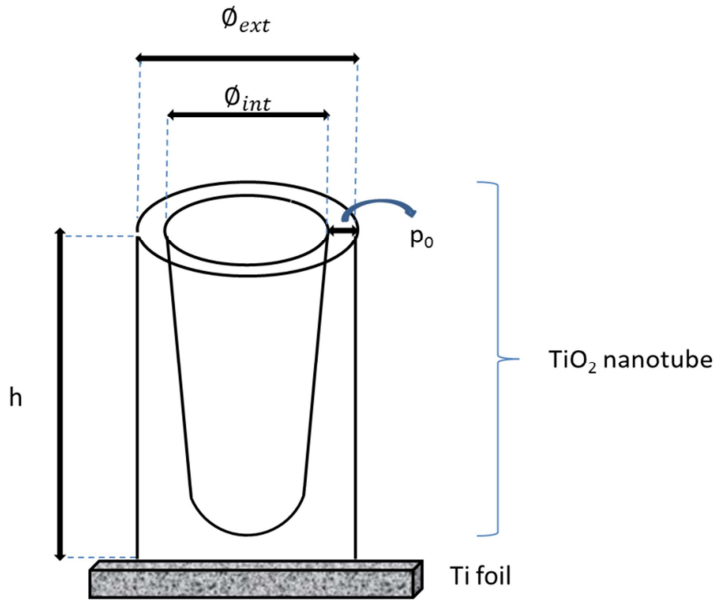

Scheme S1. Sketch for one nanotube.

A statistical analysis of top view SEM images has been done to obtain average values for the different geometric parameters of the nanotubes: external diameter ($\emptyset_{ext}$), internal diameter ($\emptyset_{int}$), length (h), and wall thickness on the top of the nanotubes (p_0). The results have been presented as ($\overline{X} \pm \text{Ɛ}$) where the average value is $\overline{X}$ and Ɛ is the corresponding error for a confidence interval of 95 %. On the other hand, σ is the standard deviation and ε_{SD} is the standard error of the average. The following equations apply:

$$\varepsilon_{SD} = \frac{\sigma}{\sqrt{N}} \qquad \text{Eq. S1}$$

$$\varepsilon = 1.96 \cdot \varepsilon_{SD} \qquad \text{Eq. S2}$$

Geometric parameters for the NTs

A total of 261 NT were measured. Scheme S2 shows the distribution of external and internal diameters.

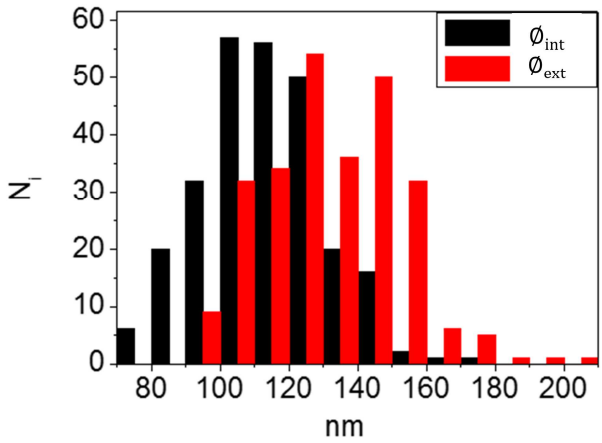

Figure S2. Distribution of internal and external diameters for the TiO_2 nanotubes as determined from an analysis of top view SEM images.

The average diameters and their standard deviation have the following values:

$$\overline{\emptyset_{int}} = 112.8 \text{ nm};\ \sigma = 17.2 \text{ nm}$$
$$\overline{\emptyset_{ext}} = 130.8\text{nm};\sigma = 18.8 \text{ nm}$$

and by employing Equation S1 and S2, the errors can be included as:

$$\overline{\emptyset_{int}} = (113 \pm 2) \text{ nm}$$
$$\overline{\emptyset_{ext}} = (131 \pm 2) \text{ nm}$$

By following a procedure similar to that described above for the NT internal and external diameters, the following values and corresponding errors were obtained for the length and wall thickness of the nanotubes:

$$\bar{h} = (3.5 \pm 0.1)\mu m$$
$$\overline{p_0} = (8.0 \pm 0.3)nm$$

TiO_2 NT surface density

Three different top-view SEM images were analyzed by counting the number of tubes per unit projected surface area and then the statistical treatment delineated above was applied for

obtaining the average surface density of the tubes and its error. A value of $(4.26 \pm 0.02) \cdot 10^9$ cm^{-2} was estimated.

TiO_2 NT volume and mass

As mentioned above, the thickness of the TiO_2 NT wall is not uniform throughout its length. It actually increases from the bottom to the top of the tubes. In order to make an accurate estimate of the tube volume, an average thickness of the NT ($\bar{p}$) can be determined as:

$$\bar{p} = \frac{\int_a^h p(h)dh}{h-a} \qquad \text{Eq. S3}$$

where the meaning of a is specified in scheme S2.

If the tube is divided into several regions as shown in scheme S2, $\bar{p}$ could be calculated as a summation of the average thickness of each region multiplied by its length:

$$\bar{p} = \frac{p_0 \cdot L_0 + p_1 \cdot L_1 + p_2 \cdot L_2 + p_3 \cdot L_3 + p_4 \cdot L_4}{L_0 + L_1 + L_2 + L_3 + L_4} \qquad \text{Eq. S4}$$

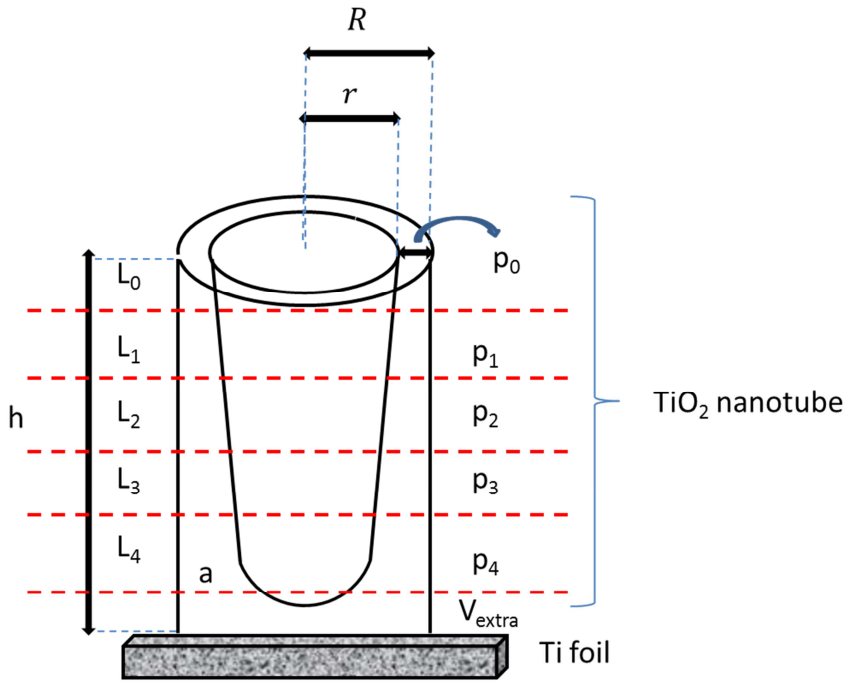

Scheme S2. Sketch showing the portions in which the NTs are divided for the sake of obtaining an average value of the NT wall thickness.

By analyzing TEM images of various tubes and by applying eq. S4, an average value of 14.2 nm is obtained for the wall thickness, which is equivalent to a value $1.78\overline{p_0}$.

The calculation of the volume of one nanotube is done by dividing it into two contributions, one associated with the walls (V) and the other with the NT bottom (V_{ext}):

$$V_t = V + V_{ext} \qquad \text{Eq. S5}$$

The first contribution can be calculated as:

$$V = \pi(R^2 - r^2)h \qquad \text{Eq. S6}$$

where R and r are respectively the external ($\frac{\emptyset_{ext}}{2}$) and the internal radius ($\frac{\emptyset_{int}}{2}$). Moreover, as $= R - \bar{p}$, Eq. S6 can be rewritten as:

$$V = \pi[R^2 - (R - \bar{p})^2]h = \pi(2R\bar{p} - \bar{p}^2)h \qquad \text{Eq. S7}$$

The second contribution can be calculated by taking into account the TiO_2 wall thickness (h_{ext}) at the bottom of the nanotubes as determined from TEM images:

$$V_{extra} = \pi R^2 h_{ext} \qquad \text{Eq. S8}$$

If we consider all the average values as determined above, the resulting average volume for one NT results to be $V_t = 2.08 \cdot 10^{-14}\text{cm}^3$. Finally, the mass per unit electrode area ($\bar{m}$) has been calculated by considering the number of tubes per cm^2, the density of amorphous TiO_2 ($\rho = 3.8 \pm 0.1\ \text{g} \cdot \text{cm}^{-3}$) and the volume of one tube:

$$\bar{m} = \bar{N} \cdot \rho \cdot V_t \qquad \text{Eq. S9}$$
$$\bar{m} = 3.36 \cdot 10^{-4}\text{g} \cdot \text{cm}^{-2}$$

On the other hand, the error made in the estimation of the nanotube volume and electrode mass density has been calculated according to:

$$\frac{\varepsilon_{V_t}}{V_t} = \frac{\varepsilon_R}{R} + \frac{\varepsilon_{p_0}}{p_0} + \frac{\varepsilon_h}{h} \qquad \text{Eq. S10}$$

where it is implicitly assumed that the main contribution to the volume comes from the term $2\pi R\overline{ph}$ and

$$\frac{\varepsilon_{\bar{m}}}{\bar{m}} = \frac{\varepsilon_N}{N} + \frac{\varepsilon_\rho}{\rho} + \frac{\varepsilon_{V_t}}{V_t} \qquad \text{Eq. S11}$$

The following value is obtained for the mass loading per unit area:

$$\bar{m} = (0.34 \pm 0.04)\ \text{mg} \cdot \text{cm}^{-2}$$

Finally, the gravimetric capacity of the electrodes has been calculated from the current used in the galvanostatic experiment (I), the charge or discharge time (t) and the mass of electrode active material (m) as:

$$C = \frac{\frac{I \cdot t}{\text{mA} \cdot \text{h}}}{\frac{\bar{m}}{\text{g}}} \qquad \text{Eq. S12}$$

With an error estimated as:

$$\varepsilon_C \cong \frac{\varepsilon_{\bar{m}}}{\bar{m}} C = 0.12 \cdot C$$

that has been employed in the error bars appearing in Fig. 3.

It is worth noting that the determination of the gravimetric capacity of the electrodes is frequently affected by relatively large errors coming from uncertainties in the electrode active mass determination. This is particularly important in the cases in which the active material is prepared by anodization. Given the low value of the mass loading typical of the electrodes employed for research, relative errors over 5-10% should be common.

Comparison of the NT behavior for two conventional organic sodium electrolytes

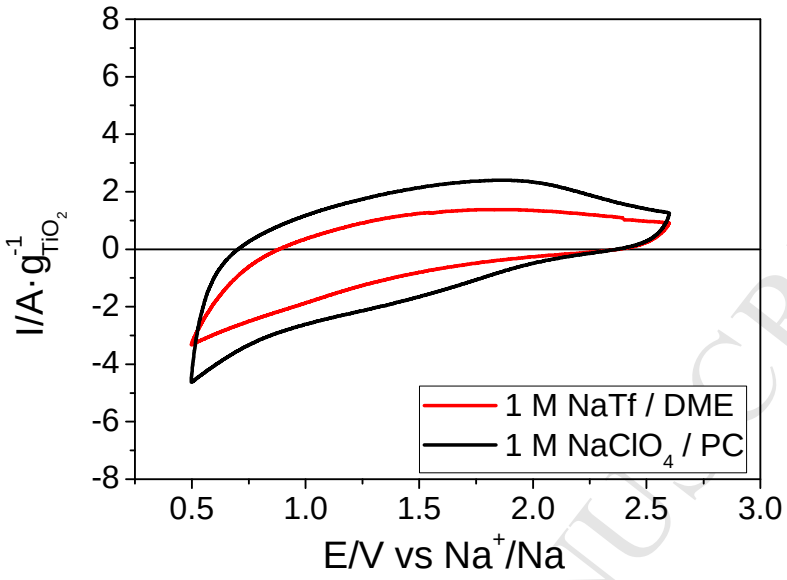

Figure S3. Cyclic voltammograms obtained for TiO_2 nanotube electrodes prepared by anodization (1 h at 40 V in the presence of 0.15 M NH_4F) in contact with either 1 M $NaClO_4$ in propylene carbonate or 1 M sodium trifluoromethanesulfonate (NaTf) in dimethoxyethane (DME). Scan rate: 10 mV·s^{-1}.

As observed, the voltammetric response in the NaTf solution is clearly inferior to that found in the $NaClO_4$ electrolyte, which is could be linked in part to the lower conductivity of the former. More importantly, problems associated with an incomplete wetting of the inner electrode surface area probably play a role.

TiO_2 NT lengths in function of different anodization times

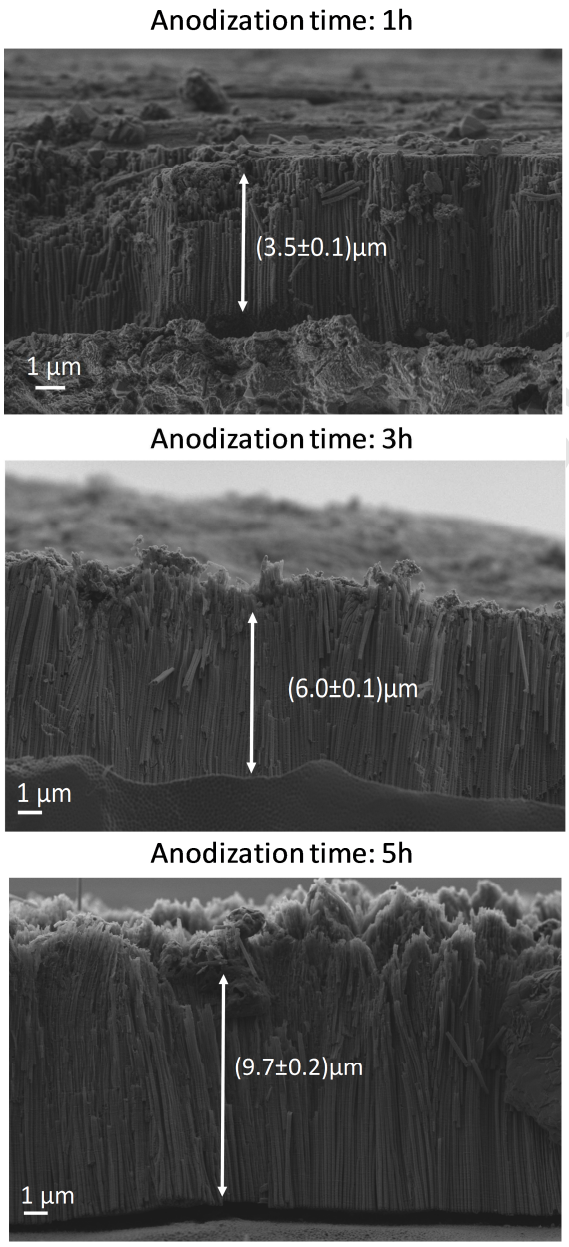

Figure S4. Variation of the TiO_2NT length in function of the anodization time. As observed from the images, the TiO_2NT length increases in function of the anodization time.

TiO_2NT electrodes darkness after sodium insertion

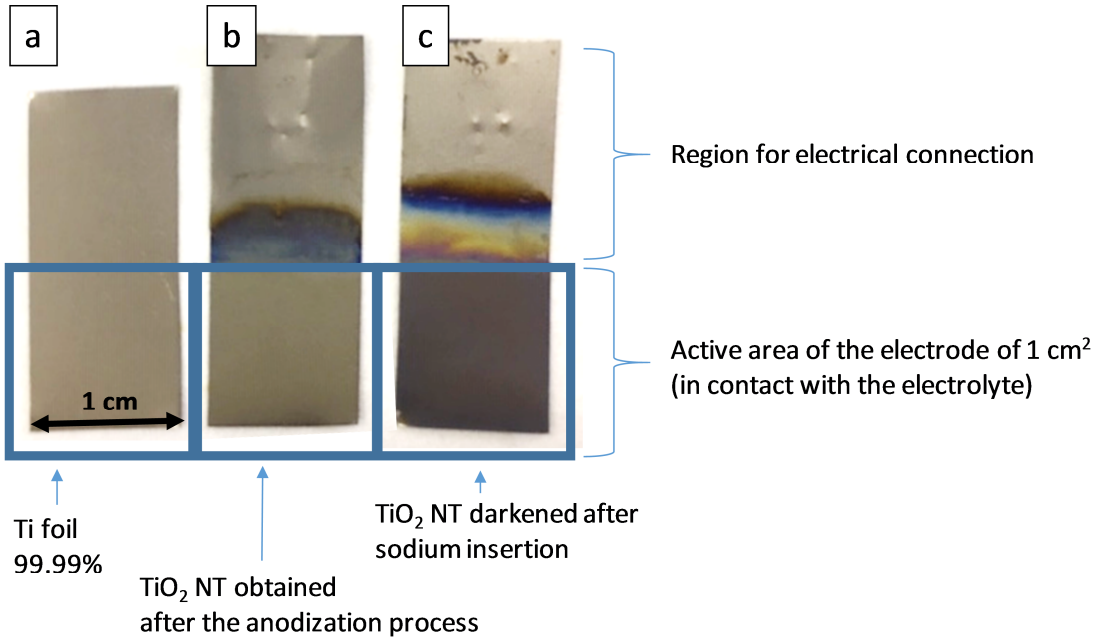

Figure S5. (a) Ti foil, (b) TiO_2NT obtained after the anodization process, (c) TiO_2NT darkened after sodium insertion. As observed from the figure, the sodiated electrode (c) shows a darkening with respect to the electrode (b) which is stable for weeks even after to exposure to the air.

As it is said in the main manuscript, the permanent darkening in the TiO_2NT electrode is associated with a irreversible reduction of some Ti(IV) atoms.

Comparison in the contact angle between 1 M $NaClO_4$/PC and $NaI \cdot 3.3NH_3$

Substrate	1 M $NaClO_4$ / PC	Saturated $NaClO_4$/ PC	$NaI \cdot 3.3NH_3$
Ti foil	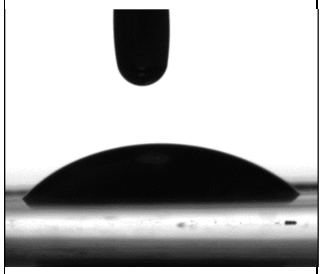 45 ± 2	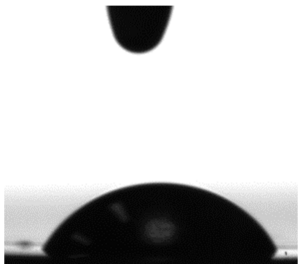 64 ± 2	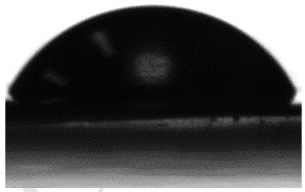 68 ± 2
TiO_2	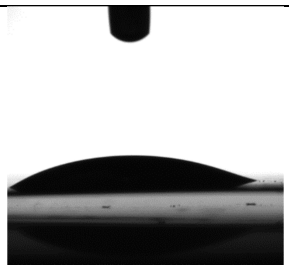 15 ± 1	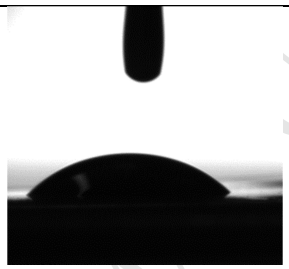 47 ± 2	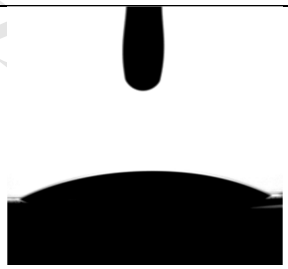 27 ± 2
NTs-TiO_2	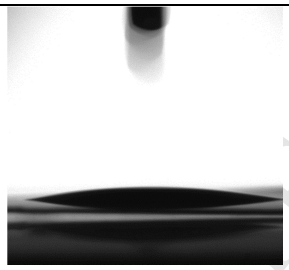 12 ± 2	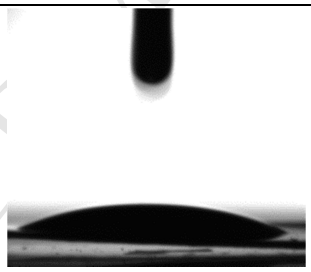 20 ± 2	 19 ± 2

Table S1. The table shows pictures as well as the values of contact angles for different solutions and substrates. Solutions: 1 M $NaClO_4$ and saturated $NaClO_4$ solutions in propylene carbonate (PC) and $NaI \cdot 3.3NH_3$. Substrates: Ti foil, TiO_2 (Ti foil heated at 450 ^{0}C in air for 1h) and, NTs-TiO_2 anodized 1h at 40 V in 0.25 M of NH_4F. The experiments were done using a KSV CAM 101 optical contact angle meter.

As observed, there is a significant difference between the contact angles obtained for 1 M $NaClO_4$/PC and $NaI \cdot 3.3NH_3$. However, the values are much closer when the ammoniate is compared to a saturated $NaClO_4$/PC solution.

Electrochemical behavior of a carbon-based electrode in $NaI \cdot 3.3NH_3$ and 1 M $NaClO_4$/PC.

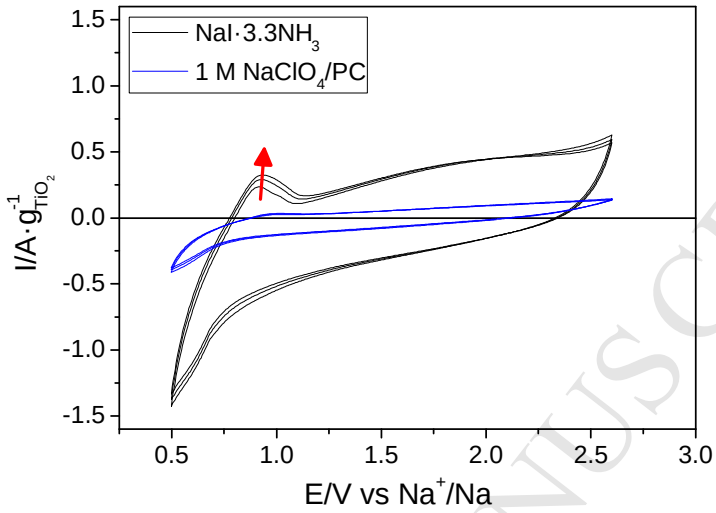

Figure S6. Cyclic voltammograms for a carbon-based electrode at 10 $mV \cdot s^{-1}$ in $NaI \cdot 3.3NH_3$ (voltammograms drawn in black, it is shown the cycle from 7 to 10, the latter two are consistent) and 1 M $NaClO_4$/PC (voltammograms drawn in blue, it is shown the cycle from 7 to 10). The working electrode was prepared by the drop casting technique from a slurry in NMP (1-methyl-2-pirrolidinone) of 70 wt% of rGO, 20 wt% of graphite power and 10 wt% of PVDF, Al covered with carbon was employed as substrate. The experiments were performed at room temperature in a two-electrode Split cell using a metallic sodium piece as a reference and counter electrode.

Working potential window for $NaI \cdot 3.3NH_3$

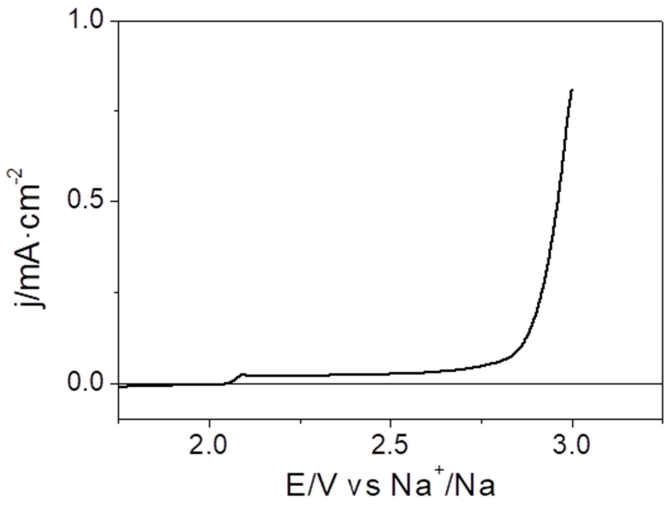

Figure S7. Positive-going voltammetric scan at 5 $mV \cdot s^{-1}$ performed for determining the working potential window (positive limit) of $NaI \cdot 3.3NH_3$. The experiment was performed in a three electrode cell using carbon-covered aluminum foil as a working electrode and metallic sodium pieces as reference and counter electrodes.

As observed, the positive limit can reach 2.8 V vs. Na^+/Na. Aluminum covered with carbon was chosen as a substrate because it is the most employed in the literature in the context of battery and, moreover, it is lightweight and cost-effective. However, it should be free of pores and scratches to avoid direct exposure of Al and its oxidation (see small signal appearing for potentials above 2.0 V).